SIMULATION OF WORKPIECE DEFORMATION CAUSED BY RELEASING THE CLAMPING FORCE

Xiao-Dong Shao[1], Si-Meng Liu[1] Liu Zhang[2] and Zhao-Xu Lin[1]
[1]*Key Laboratory of Electronic Equipment Structure Design, Ministry of Education, School of Mechano-Electronic Engineering, XiDian University, Xi'An 710071, China*
[2]*The 14th Research Institute of CETC, NanJing 200013, China*
E-mail: shao_xiao_dong@163.com; lemonlsm@sohu.com

ICETI-J1054_SCI
No. 13-CSME-56, E.I.C. Accession 3514

ABSTRACT
A novel algorithm to predict machining error caused by releasing the clamping force is put forward in this paper. First, the deformity of the workpiece by clamping force is calculated using FEM. Then the relaxing deformity of the workpiece caused by releasing the clamping force is calculated by the mapping method based on mesh model. The machining error is achieved using error analysis technology. A test is conducted to verify the performance of the simulation result.

Keywords: clamping force; error; simulation; finite element method.

SIMULATION DE LA DÉFORMATION DES PIÈCES PROVOQUÉE PAR LA FORCE DE SERRAGE

RÉSUMÉ
Cet article propose un algorithme pour prédire l'erreur d'usinage provoquée par la détente de la force de serrage. La méthode des éléments finis est d'abord utilisée pour calculer la déformation des pièces par la force de serrage. Ensuite, la difformité causée par la détente de la force sur la pièce est calculée par cartographie en se basant sur un modèle maillé. L'erreur d'usinage est obtenue en utilisant la technologie d'analyse d'erreur. On procède au test de l'algorithme pour vérifier la performance du modèle de simulation.

Mots-clés : force de serrage ; erreur ; simulation ; méthode des éléments finis.

1. INTRODUCTION

Machining error caused by clamping force is a vital factor in finish machining. Studies [1–3] show that machining error caused by clamping force mainly comes from three aspects. Firstly, insufficient clamping force can make the workpiece slip and vibrate during processing, which causes machining error and can even damage the workpiece and cutting tool. Secondly, in the process of clamping, due to improper sequence or uneven clamping force, the located workpiece deviates from the ideal location and angle which results in machining error. Thirdly, the workpiece deforms elastically owing to clamping force. Once the force is removed after processing, it causes springback deformation (as shown in Fig. 2). This will result in the workpiece being measured accurately at the clamping state, but exceeding the specified dimensions after the clamp is released.

The studies of clamping error mainly focus on the minimum clamping force and the best clamping sequence. The former solves the problem by setting the clamping force reasonably. The research of De Meter et al. [1] shows that too small a clamping force will cause vibration and slippage of the workpiece, while too large a clamping force will cause non-negligible elastic deformation. Both cases will lead to lower processing quality. Therefore there is a need to calculate the minimum clamping force which is required for steady clamping, and to give the minimum preload prediction model. Jeng et al. [2] study the minimum clamping force by using the instantaneous center of motion (ICM). By calculating the ICM of the fixture-workpiece system, the minimum clamping force is calculated according to the balance between the cutting moment and the clamping friction moment. The latter achieves more accurate positioning by establishing a reasonable order of clamping. Raghu and Melkote [3] discuss the case of modular fixture in different clamping sequences, the deviation of positioning and its effects on machining error.

In the current study of clamping error, research of the third category mainly focus on the calculation of the minimum clamping force. There is less work on the springback deformation and the quantitative calculation of machining error. This paper conducts a study of the problem, and sets up an analysis model of springback and the machining error it causes. We call this kind of error as clamping released error. Moreover, solutions to the key technology are studied.

2. MACHINING ERRORS SIMULATION

2.1. Machining Errors Model

Figure 1 shows a typical project in which machining precision is affected by clamping force: clamping the base and cylindrical part by modular fixture, then processing the inner circular hole. The inspection result indicates that the precision of the hole under clamping state meets the design requirements after finishing, but when the fixture is removed, the errors increase and the roundness deviation of some of the workpieces exceed the limit.

Figure 2 shows the formation process of clamping released errors during hole processing. Figure 2a is the work-blank, the inner circular hole of which will be milled. The clamping force needs to be applied in both sides of the work-blank to ensure the stability of the process. The workpiece has elastic deformation because of the clamping force, as shown in Fig. 2b. Assuming the cutting force, vibration, cutting caloric, tool wear, machine error, fixture positioning errors and other factors are ignored, the machined surface should be an ideal hole as shown in Fig. 2c after cutting. The workpiece rebounds and the machined surface deforms due to the release of the clamping force as shown in Fig. 2d, which leads the machining error.

The workpiece is in two states in the process shown in Fig. 2, one is the clamping state of being applied with clamping force, and the other is the free state with the clamping force released. Given the known shape of the workpiece in the initial free state, the mesh model W_0 of the workpiece in the free state is available by finite element mesh generation. After applying the clamping force F and constraint to W_0, the mesh model W_1 of the deformed workpiece in the clamping state can be obtained by finite element method. Then the

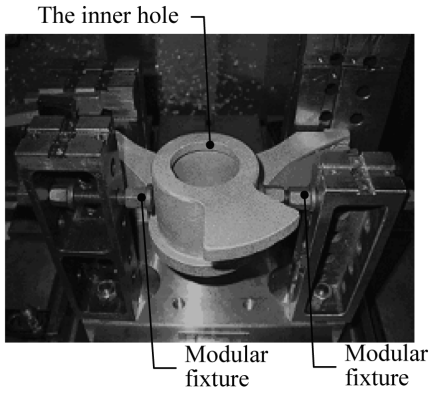

Fig. 1. The case of accuracy affected by the clamping force.

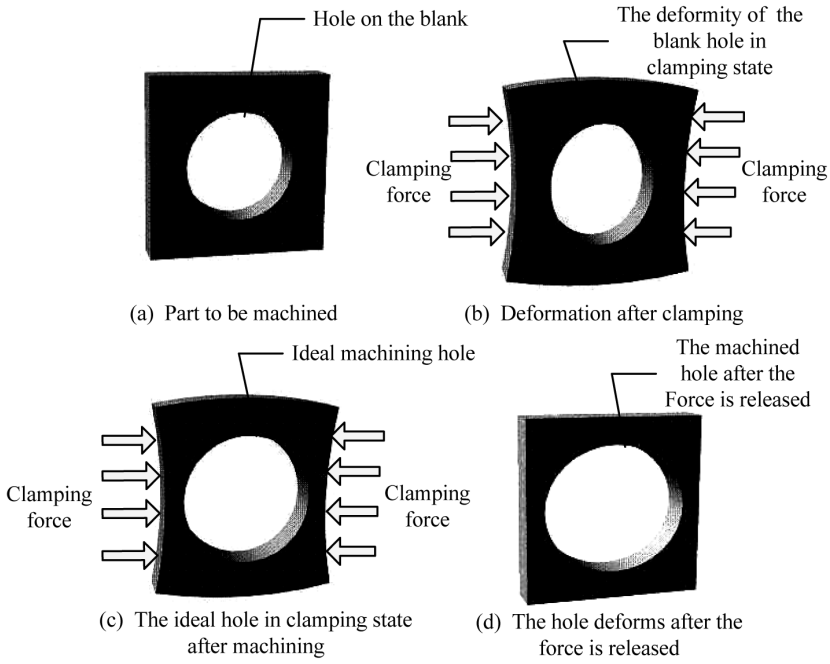

Fig. 2. Machining error caused by the clamping force.

finished machined face profile $Face_1$ and the sampling points $Verts_1$ of $Face_1$ in the clamping state can be obtained by the analysis of the tool path. The problem which is to be solved is the clamping error after the clamp is released.

2.2. Key Techniques

In the simulation models of the clamping released error described previously, the calculation of the clamped workpiece mesh model W_1, the machined surface in the free state W_0, and the machining errors are the key techniques to master.

2.2.1. The Calculation of the Grid Model

The foundation of the grid model is based on the structure and shape of the workpiece. It can be divided artificially to improve the quality of the grid model. For a workpiece with simple shape, it can be divided di-

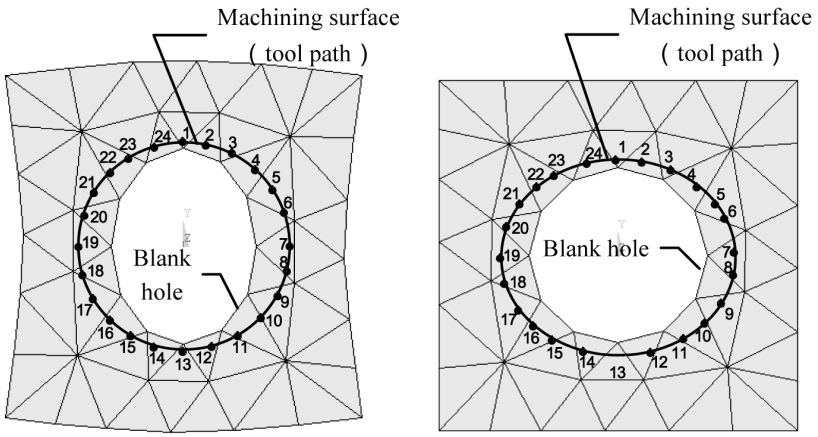

(a) The grid model in clamping state (b) The grid model in free state

Fig. 3. The variation of track points in the grid model before and after releasing the clamping force.

rectly by mature finite element software. The finite element modeling and calculation is finished by ANSYS as demonstrated in the paper. Firstly, mesh the geometric model with tetrahedron element. Secondly, make the force F equal to a uniformly distributed load along the contact area of the fixture and the workpiece. Finally, set the fixture as fixed-end constraint and the element on the contact surface of fixture and workpiece as contact element. Contact element is a special element type in Ansys, which can effectively simulate the constraint relationship of the fixture and the workpiece. The output state variable *Stat* of the element represents the relative status between the contact surfaces. When $Stat \leq 1$, the contact surface is on a separate state, $1 \leq Stat \leq 2$ indicates that the two contact surfaces have relative sliding, $2 \leq Stat \leq 3$ indicates that the two contact surfaces are closely attached. It can be determined whether the given clamping force can ensure steady clamping. Finally, call the Ansys model solver function to complete the deformation calculation, and export mesh model W_0 in the free state and the mesh model W_1 in the clamping state.

2.2.2. Calculation of the Shape of the Machined Surface in the Free State

(1) Basic approach The calculation of the machined surface F_0 after releasing the clamping force is key to the whole clamping released error simulation algorithm. According to finite element theory, W_0 is similar in topology to one of the workpiece after deformation. In other words, the difference is only on the node coordinates, while the quantity, the number and the connection relations are identical (shown in Fig. 3). Meanwhile, the position of $Verts_1$ and $Verts_0$ in the mesh model is also similar in topology. That is, there are similarities in the position in grid W_1 and W_0 of any set of corresponding points in the tool track points set. As shown in Fig. 3a, the position of the tool track point number 1 to number 24 in grid W_1 is similar to that of the corresponding points in grid W_0 shown in Fig. 3b.

Based on the above analysis, this paper presents the basic idea of the $Face_0$ calculation algorithm. According to the principle of the invariant grid position of the tool track points in clamping state and free state, mapping all points in set $Verts_1 \in Face_1$ from W_1 to W_0 will form the sampling points set $Verts_0$ of machining face in the free state. The machining face $Face_0$ in the free state can then be obtained with the reasonable surface fitting method.

(2) $Verts_1$ acquisition The finished surface $Face_1$ in clamping state is actually formed by the space track which the cutting edge goes by. For the ideal processing state with vibration, cutting force and other influencing factors being neglected, the cutter spacing control points in NC program are actually a set of discrete

points on Face_1. Verts_1 can be obtained through analysis of the NC program. Also, it can be gained by means of detection of the finished surface which is in clamping state after processing. For the case which is shown in Fig. 1, the calculation of the set of discrete points is much simpler. Since the tool orbits along the axis of the hole, we can take N_z sampling circles along the axis, and N_o sampling points on each circle circumferentially to get the set of sampling points. The formulas of the ith sampling point P_i are

$$\left\{\begin{array}{l} m = \text{mod}(i, N_o) \\ x_i = x_0 + R * \cos(m * 360/N_o) \\ y_i = y_0 + R * \sin(m * 360/N_o) \\ z_i = z_0 + (L/N_z) * \text{div}(i, N_o) \end{array}\right\} \tag{1}$$

where R is the radius of gyration of the tool, L is the axial length of processing of the hole, (x_0, y_0, z_0) are the coordinates of the rotation center of the tool, $i = 1, \ldots, N_o * N_z$, and mod is the complementation function, div is the divisible function.

(3) The principle of which the tool track points' position is constant in the grid model Set W_0 as the grid model in the free state, and W_1 as the grid model in the clamping state. P_1 is an arbitrary point in the W_1 space, Cell_P_1 is the element where P_1 lays, and No_Cell_P_1 is the element number. P_0 is the mapping point of P_1 when the workpiece bounces back from W_1 to W_0, Cell_P_0 is the element where P_0 lays, and No_Cell_P_0 is the element number. The rules are as follows: (1) the grid cell in which the points are located does not change after mapping, that is $\text{No\_Cell\_P}_1 = \text{No\_Cell\_P}_0$; and (2) the points are similar in location within their elements after mapping, the similarity can be expressed by

$$K_i^1 = K_i^0 \quad (i = 1, \ldots, 4) \tag{2}$$

$$K_i^1 = |P_1, F_i^1| / |V_i^1, F_i^1| \tag{3}$$

$$K_i^0 = |P_0, F_i^0| / |V_i^0, F_i^0| \tag{4}$$

where the meaning of V_i^1, F_i^1, V_i^0 and F_i^0 is shown in Fig. 4. V_i^1 represents the four vertexes of the tetrahedral element CELL_P_1, F_i^1 is the undersurface which corresponds to V_i^0. V_i^0 and F_i^0 are the vertex and undersurface of CELL_P_0. $|P_1, F_i^1|$ is the distance from the point P_1 to the surface F_i^1, $|V_i^1,\ F_i^1|$ is the distance from each vertex V_i^1 to the corresponding surface F_i^1. The meaning of $|P_0,\ F_i^0|$ and $|V_i^0,\ F_i^0|$ is similar.

Eqs. (2)–(4) indicate that there is similarity in the position of P_1 in CELL_P_1 and P_0 in CELL_P_0.

(4) The vertex mapping arithmetic based on grid The mapping algorithm to Verts_1 is achieved based on the above principles. Figure 5 shows the algorithm flow of which the arbitrary point P_1 in Verts_1 maps from space W_1 to W_0. Verts_0 can be obtained by transferring all points in Verts_1 to W_0.

The algorithm shown in Fig. 5 contains two problems, one is calculating Cell_P_1 and Cell_P_0, and the other is seeking P_0 by P_1 and Cell_P_1 and Cell_P_0.

1. Confirm Cell_P_1 and Cell_P_0

   Calculate Cell_P_1, a grid cell in W_1, in which P_1 exists. The results can be obtained by discriminating all cells in W_1.

   Rule to discriminate whether the point P exists in the element Cell: in the tetrahedron element Cell as shown in Fig. 6, for the point and area set $\{\text{V}_i, \text{F}_i \mid i = 1, \ldots, 4\}$, if there is any set of (V_i, F_i) in which the point P and point V_i are separately on both sides of the plane F_i, then the point P is on the outside

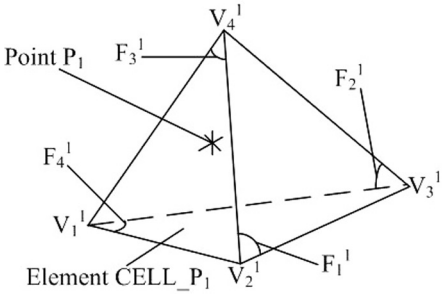

(a) The element Cell_P_1 where P_1 lays in the clamping state

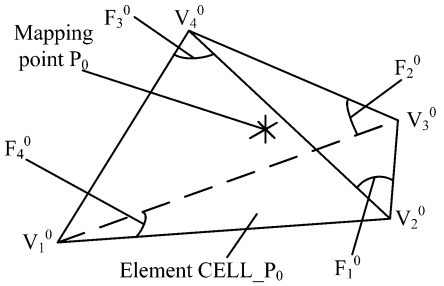

(b) The element Cell_P_0 where P_0 lays in the free state

Fig. 4. The tool track points' position is constant in the grid model.

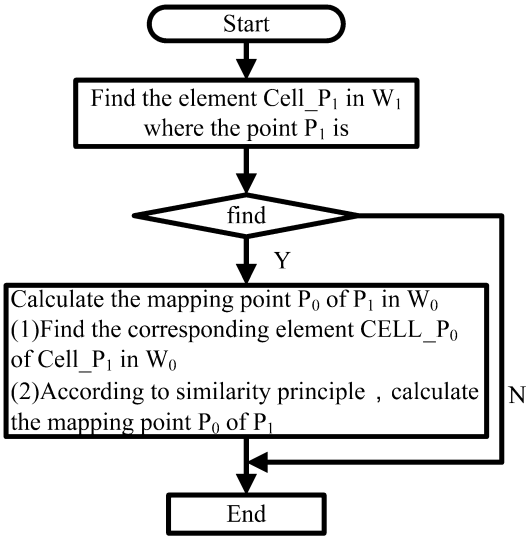

Fig. 5. The mapping algorithm to arbitrary point P1 based on grid.

of the element Cell, otherwise the point P is in the element. This can be expressed by the following formula:

$$\left\{\begin{array}{l} \mathrm{dis}(P,F_i)*\mathrm{dis}(V_i,F_i)>0 \quad (i=1,\ldots,4) \\ \mathrm{dis}(P,F_i)=\mathrm{SIGNAL}(A_i*X_p+B_i*Y_p+C_i*Z_p+D_i) \\ \mathrm{dis}(V_i,F_i)=\mathrm{SIGNAL}(A_i*X_{V_i}+B_i*Y_{V_i}+C_i*Z_{V_i}+D_i) \end{array}\right\} \tag{5}$$

where the plane equation of F_i is $A_i*\mathrm{X}+B_i*\mathrm{Y}+C_i*\mathrm{Z}+D_i$, SIGNAL is sign function, dis is the

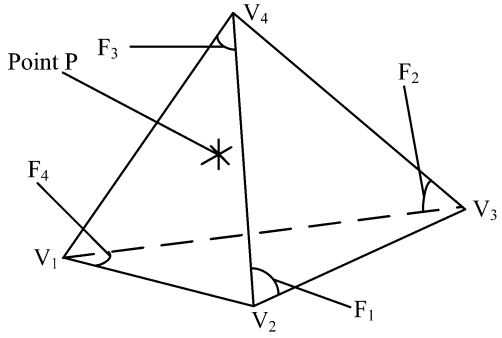

Fig. 6. The discrimination of the relative relation of point P and tetrahedron CELL.

distance function of an indicated point to an indicated plane. X_p and Y_p and Z_p are coordinates of the point P, X_{Vi} and Y_{Vi} and Z_{Vi} are coordinates of the point V_i.

When we get CELL_P_1, according to the principle of No_Cell_P_0 = No_Cell_P_1, the element Cell_P_0 where P_0 lays can be found in W_0.

2. Calculation of P_0

The tetrahedral mapping algorithm flow of the point P_1 is shown in Fig. 7. First, calculate the distance coefficients K_1^1, K_2^1, K_3^1 of the point P_1 which is in the element CELL_P_1 according to Eq. (3). And we get $K_1^0 = K_1^1$, $K_2^0 = K_2^1$, $K_3^0 = K_3^1$ according to Eq. (2). Then the distance d_1^0, d_2^0 and d_3^0 of the point P_0 to the three surface F_1^0, F_2^0 and F_3^0 of CELL_P_0 can be obtained according to Eq. (4). Establish parallel faces FP_1^0, FP_2^0 and FP_3^0 of F_1^0, F_2^0 and F_3^0, and the distance of each pair of parallel faces are d_1^0, d_2^0 and d_3^0 respectively. Then determine the intersection point of FP_1^0, FP_2^0 and FP_3^0 to get the mapping point P_0 of point P_1. Figure 7 shows that parPlane(d,F) represents the plane which is parallel to plane F, and the distance between the two planes is d. intPlane(FP_1, FP_2, and FP_3) represents the intersection point of FP_1, FP_2, and FP_3.

Mapping all the processing track points in turn in the set $Verts_1$ according to the algorithm which is shown in Fig. 7 will enable the acquisition of the set of processing track points $Verts_0$ after the release of the clamping force.

2.2.3. Calculation of Machining Error

The machining error can be obtained by further processing $Verts_0$. The following are the basic steps. First get the interpolation surface of $Verts_0$, i.e. $Face_0$ after the workpiece springs back. And according to the definition of various kinds of machining errors, the simulation result of machining error is obtained by the calculation of the ideal surface and actual surface of the workpiece. This paper will not discuss the calculation of machining error in depth [4].

3. EXPERIMENTAL VERIFICATION

In order to verify the performance of the presented simulation algorithm, we carry out an experiment. The structure which is used to verify the workpiece is shown in Fig. 8a. In order to minimize the impact of other factors, we chose the simplest cylindrical workpiece to process its inner hole. The hole diameter of the work-blank is 61.378 mm, the size after processing becomes 61.428 mm. The material is cast aluminum. The clamping force chosen in the experiment is 10 KN (in the normal case of clamping, the force is a few Newton to dozens of Newton), this was used to produce the greatest possible clamping deformation in order to eliminate the influence of other factors on the simulation result of clamping errors.

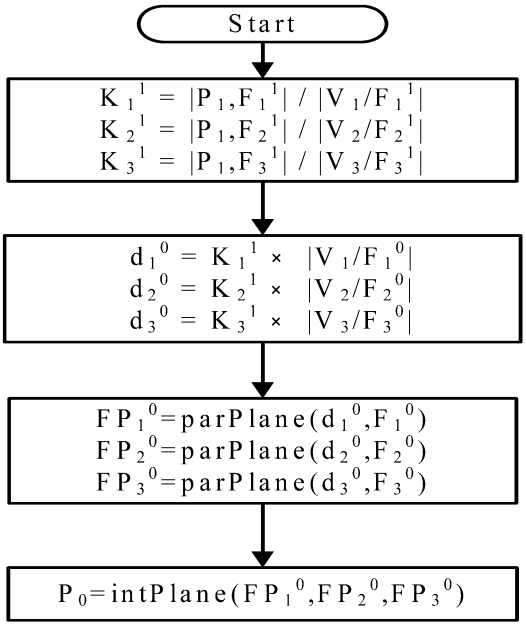

Fig. 7. The tetrahedral mapping algorithm flow of the point P1.

Table 1. Comparison of the sampling values of the machining face and the simulation results before and after the clamping is released.

Ideal points (before the clamping is released)			Test value (after the clamping is released)			Simulation value (after the clamping is released)		
x/mm	y/mm	z/mm	x/mm	y/mm	z/mm	x/mm	y/mm	z/mm
30.714	0	–9	30.522	0.008	–9.002	30.538	0.1559	–9.0027
28.376	11.754	–9	28.244	11.689	–9	28.224	11.929	–9.0032
21.718	21.718	–9	21.667	21.728	–9.001	21.621	21.938	–9.0042
				.....				
30.714	0	–29	30.534	–0.003	–29.002	30.557	0.154	–29.0006
28.376	11.754	–29	28.257	11.695	–29	28.238	11.926	–29.0007
21.718	21.718	–29	21.676	21.738	–29	21.628	21.932	–29.0016
				.....				
cylindricity			0.301mm			0.3508mm		

In order to make the shape of the surface close to an ideal circle after machining, a semi-finished workpiece is chosen as the work-blank for finish milling. The machine tool is UCP710 CNC controlled 5-Axis machining center, of which the spindle speed is 800 rpm, the cutting speed is 30 mm/min, and the amount of feed is 0.025 mm. After the machining is finished and before the clamping is removed, measuring with the lever gauge (the μ gauge) in various locations show between $Z = -9$ mm and $Z = -29$ mm, and the pointer does not move, which indicates that in the clamping state after finish milling, the hole is close to the ideal shape. The clamping is then removed, and the hole is again measured with the three-coordinate measuring machine. The result shows that there is machining error, which is shown in Table 1.

Simulation of clamping error is carried out on the workpiece as shown in Fig. 8a with the above simulation algorithm. First, the geometry model (Fig. 8b) is constructed and the finite element model (Fig. 8c) is meshed for the workpiece. The material density, Young modulus and Poisson ratio are set as 2660 kg/m^3, 76E9Pa and 0.33 respectively. The clamping load is set as a distributed force, of which the size is 10 KN. The

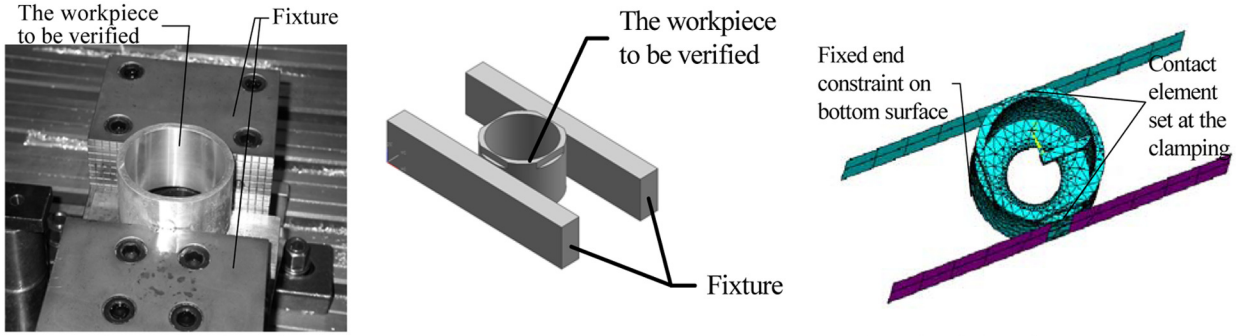

(a) The actual clamping situation (b) The geometric model (c) The finite element model

Fig. 8. The workpiece for verification.

deformation of the workpiece produced by the clamping force is obtained and outputted as the grid model W_1 after resolving. Next, get $Verts_1$ by the ideal machining path. Finally, after vertex mapping and error analysis, the simulation result of machining error is available (Table 1).

It can be seen in Table 1 that for the verification case, the measured value of clamping error (cylindricity) is 0.301 mm, and the simulation value is 0.3508 mm. The experimental results are smaller than the simulation results. There are three reasons which can lead to the difference of results. First, it is assumed in the simulation that the machining face in the clamping state after processing is an ideal circle, while there always exists errors on the machining face during the experiment. Second, there is deviation between clamping deformation FEM and the actual model. Third, there is a certain amount of error in the coordinate measuring device.

4. CONCLUSION

The proposed algorithm of clamping released error simulation achieves the deformation caused by clamping force with FEM, calculates the springback deformation of the machined surface using grid mapping method, and obtains the machining error by error analysis. Experiment shows that the test value is consistent with the simulation value, which proves the effectiveness of the algorithm.

Study on how to reduce the clamping released error is of great importance to improve the accuracy of precision machining. Both the simulation and experiment indicate that, in the case of common processing, the clamping released error is from 0.1 to 0.8 microns while the error induced by the other factors such as cutting force, vibration, cutting heat, tool wear is more than 10 microns. Therefore, the effect of clamping released error on the whole is insignificant and can be ignored. However, in the case of finish machining such as finish milling, the clamping released error significantly impacts on the final error of the workpiece and must be considered because the machining accuracy before the fixture is released can reach about 1 micron. According to the literatures available, there is no other research on the clamping released error simulation.

Based on the work of this paper, one can minimize clamping released error by improving the manufacturing setup planning and the tool path. For example, one can optimize the clamping force and location points under the condition of stable clamping. One can also design the tool path as a non-ideal surface under the clamping condition and achieve the ideal machining face after the clamping force is released and the workpiece springs back. Further related research will be done in future studies.

REFERENCES

1. De Meter, E.C., Xie, W., Choudhuri, S., et al., "A model to predict minimum required clamp pre-loads in light of fixture-workpiece compliance", *International Journal of Machine Tools & Manufacture*, Vol. 41, No. 7, pp. 1031–1054, 2001.
2. Jeng, S.-L., Chen, L.-J. and Chieng, W.-H., "Analysis of minimum clamping force", *International Journal of Machine Tools & Manufacture*, Vol. 35, No. 9, pp. 1213–1224, 1995.
3. Raghu, A. and Melkote, S.N., "Analysis of the effects of fixture clamping sequence on part location errors", *International Journal of Machine Tools & Manufacture*, Vol. 44, No. 4, pp. 373–382, 2004.
4. Shao, X.D., Wang, H.Z. and Lin, Z.X., "Study on error analysis of visual manufacturing process by physical simulation", *Electro-Mechanical Engineering*, Vol. 22, No. 2, pp. 56–59, 2006 [in Chinese].